

# Application of Spectral Decomposition to Detect Deepwater Gas Reservoir

Ji-Xin Deng<sup>\*1,2</sup>, De-Hua Han<sup>2</sup>, Jiajin Liu<sup>2</sup> and Qiuliang Yao<sup>2</sup>

<sup>1</sup>College of Information Engineering, Chengdu University of Technology

<sup>2</sup>Rock Physics Lab, University of Houston

## Summary

In this paper, spectral decomposition techniques are applied to deepwater seismic data from Gulf of Mexico to examine the gas associated spectral anomalies. In the first case, thick gas sand with nearly constant P-impedance is encased in shale with non-symmetric P-impedance, and gas reservoir are bright at low-frequency iso-frequency sections; Commercial gas sand and low-gas saturated sand also show apparently different spectral characteristics. In the second case, gas reservoir includes two consecutive up-fining sand intervals with gradually changed P-impedance in each sand interval. Spectral anomalies of gas sand occur at high-frequency iso-frequency sections. Detailed forward modeling is analyzed to help understand the underlying physical mechanisms. Reservoir thickness and P-impedance structure are the first order factors to control the spectral decomposition responses of the above two gas reservoirs. Systematic synthetic model based on reservoir properties is needed to select optimal frequency range to directly detect hydrocarbon for specific reservoir.

## Introduction

Spectral decomposition techniques typically generate a continuous volume of instantaneous spectral attributes from broadband seismic data, to provide useful information for reservoir characterization and direct hydrocarbon detection (Partyka, et al., 1999; Castagna et al., 2003; Liu and Marfuit, 2007). Conventional spectral decomposition is performed using the discrete Fourier Transform, which is preferred for evaluating the spectral characteristics of long windows containing many events (Castagna, et al., 2006). Decreasing the time window length to increase the time resolution, the frequency resolution will be compromised. In recent years, several spectral decomposition techniques have been developed, such as instantaneous spectral analysis and exponential pursuit decomposition, to achieve better temporal and spectral resolution (Castagna, et al., 2003, 2006). In this study, S-transform is applied to deepwater seismic data from Gulf of Mexico to get different instantaneous frequency volumes. The S-transform improves spectral resolution by using variable window length as a function of frequency (Stockwell, et al., 1996). It was widely accepted that gas associated spectral anomalies often occurred at low frequency. Spectral decomposition results of gas reservoir can show low

frequency or high frequency anomalies depending on reservoir thickness and P-impedance structure.

## Reservoir Background

Figure 1 shows a 2D poststack seismic line across the King Kong minibasin from a 3D seismic data in Green Canyon of Gulf of Mexico. Reservoir in King Kong contains two gas sand intervals (Sand-1 and Sand-2 in Figure 1), which show strong amplitude anomalies with two trough/peak doublets. Later studies indicate that sand reservoir extends from CDP 3 to 45, and commercial gas sands ( $S_w < 0.3$ ) are in the CDP number from 6 to 26. The rest are mainly low-gas saturated sands ( $S_w > 0.9$ ) (Zhao, et al, 2006; Chi, et al, 2006). Commercial gas sands and low-gas saturated sands also show typical class III AVO anomalies, but commercial gas sand has relatively larger amplitude response than low-gas saturated sands in the stack section.

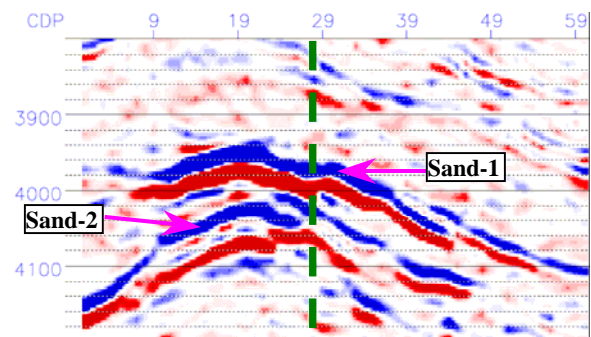


Figure 1. Broad-band stacked seismic section across King Kong showing two gas sands.

## Spectral Decomposition Properties

Figure 2 shows iso-frequency sections from the stacked seismic data using S-transform. The commercial gas zone in Sand-1 is bright at 9Hz, while the low-gas saturated sands do not exhibit apparent anomalies compared with background. But we can observe a high energy low frequency shadow under this sand layer. In 15Hz section both commercial gas sands and low-gas saturated sands stand out, and the difference between them become relatively weak. At frequency 23Hz, commercial gas zone are still brighter than the low-gas saturated zone and

## Application of Spectral Decomposition to Detect Deepwater Gas Reservoir

background. The sand layer becomes completely invisible at high frequency 40Hz section. For sand-1 reservoir, gas associated anomaly is outstanding on low frequency range.

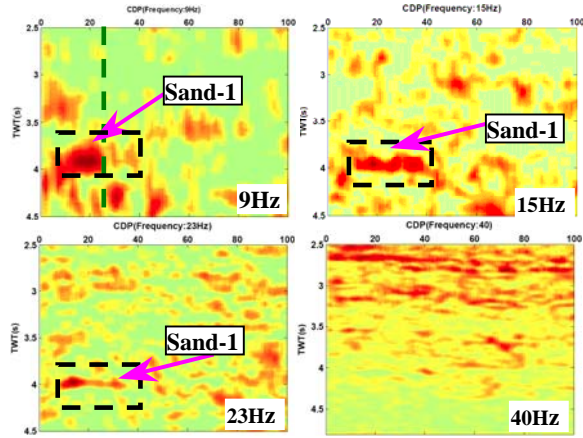


Figure 2. Selected iso-frequency sections of the stacked seismic data of King Kong.

Systematic wedge models were built to study the effects of impedance structure and layer thickness on the spectral decomposition response. Velocity and density of shale and gas sand ( $S_w=0.1$ ) were derived from reference well by using Backus' average. The P-wave impedance of underneath shale is higher than that of overlying shale (Figure 3a). Gassmann's equation was used to compute the P-wave impedance of interbedded sand at different gas saturation, where pore fluid properties are calculated using Baltze-Wang relations (Baltze and Wang, 1992) according to in situ conditions of pay sand. Synthetic seismograms of those wedge models were generated with a plane wave convolution approach, and the input wavelet is zero-phase Ricker wavelet with peak frequency of 25Hz.

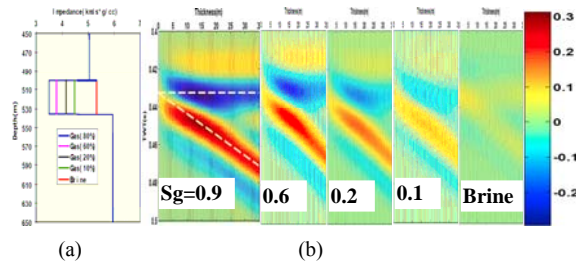


Figure3. (a)P-impedance for the wedge models; (b)Corresponding synthetic seismic response of the wedge models, where  $S_g$  is the gas saturation.

Figure 4a displays peak instantaneous frequency against sand thickness for those wedge models. Peak frequency changes complicatedly with thickness. When the sand

thickness is thinner than the tuning thickness ( $1/4$  wavelength, about 18m for sand wedge with gas saturation of 0.9), peak frequencies increase with gas concentration at same thickness, which means that peak frequencies will shift to high frequency for gas saturated sand compared with brine sand, and the maximum frequency difference is about 3.5Hz. For thick sand (larger than the tuning thickness), the peak frequencies of gas-saturated sand are lower than that of brine sand. Such phenomena can be explained in the frequency domain as the result of spectrum interference between the wavelet and reflectivity series (Partyka, et al., 1999; Chen, et al., 2006). Figure 4b shows the amplitude spectrum at wedge thickness of 22m, which is equal to the layer thickness of Sand-1. We can observe clearly that the peak frequencies of gas sands will shift to low frequency with increasing gas concentration. We also use the constant quality factor "Q" model to generate synthetic responses at the same layer thickness of 22m, the results show that peak frequency is insensitive to relative values of Quality factor (Q), and even a very small Q value will not cause visible frequency shift of reflection spectrum.

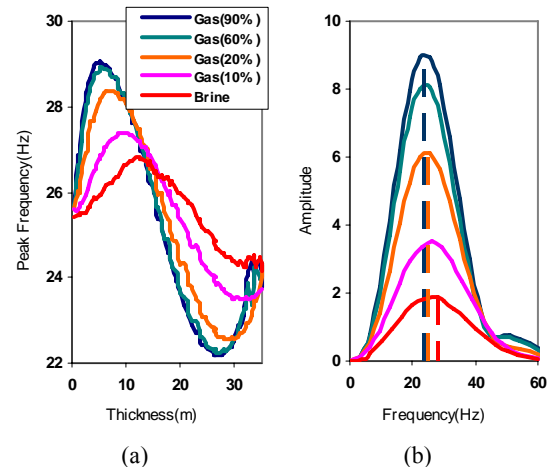


Figure 4. (a) Peak frequency versus wedge thickness for zero-degree incidence; (b)Amplitude spectrum at wedge thickness of 22m.

Figure 5 shows the spectral ratios between different gas saturation sand and brine sand at sand thickness of 22m. The spectral ratios show relative large values at certain relatively low frequency range, which indicate that brine sand and gas sand have a apparent spectral decomposition discrepancy at that frequency range. The frequency corresponding to maximum spectral ratio will increase with decreasing gas saturation, such as from 16.5Hz for gas saturation of 0.9 to about 23Hz for gas saturation of 0.1. The minimum spectral ratios for gas saturation conditions will reach at about 45Hz. At each frequency, amplitude contrast is stronger for high gas content. Those results are

## Application of Spectral Decomposition to Detect Deepwater Gas Reservoir

consistent with what we have observed in the spectral decomposition results of the seismic data (Figure 2).

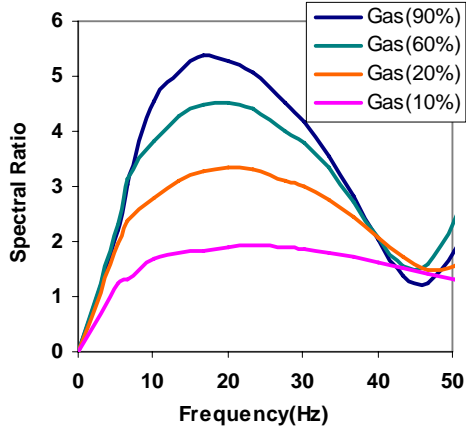


Figure 5. Spectral ratios between different gas saturation sand and brine sand at layer thickness of 22m.

In the above example, P-impedance of sand wedge keeps constant for each saturation condition, which conforms to well log measurement of Sand-1. Actually, P-impedance often shows gradual change in values for a given sand layer under deepwater sedimentary circumstance. Figure 6a shows the cross-plot of P-impedance versus porosity for the brine sand interval of a typical fining upward cycle in the reference well, superimposed on the unconsolidated line representing sorting effects with constant clay content (Dvorkin and Gutierrez, 2001). We observe an overturned V-shape for P-impedance in well log (Figure 6b), which reflects the effect of pore filling clay on the elastic properties and porosity of unconsolidated sand. Increasing pore filling clay content will reduce porosity, thus stiffen the rock, so P-impedance increases gradually from top to bottom for an up-fining sand interval.

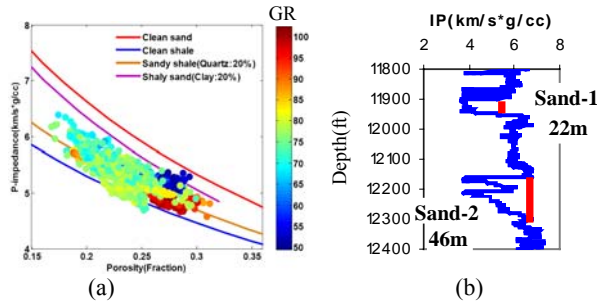


Figure 6. (a) P-impedance versus porosity for the brine sand interval in the reference well; (b) P-impedance for Sand-1 and Sand-2.

Sand-2 includes two consecutive up-fining sand intervals (Figure 6b), and the gross thickness is about 46m. Figure 7a shows the P-impedance of the wedge model containing two consecutive sand intervals with different gas saturation. In each sand transitional interval, the values of minimum impedance and maximum impedance are derived directly from the well, and P-impedance in between are linearly interpolated to mimic the impedance structure observed in the reference well. P-wave impedance of surrounding shale is also derived from the well using Backus' average. Corresponding synthetic seismograms of the wedge models for different gas saturations are shown in Figure 7b. Figure 8a displays peak frequency against gross sand thickness for different gas saturations. When the gross sand thickness is larger than 35m, the peak frequency of gas sand is apparently higher than that of brine sand. But for thickness less than that, the peak frequency differences are subtle. Figure 8 shows the spectral ratios between different gas saturation sand and brine sand at gross sand thickness of 46m. The spectral ratio is largest at high frequency range about 38Hz. The minimum spectral ratios for gas saturation conditions will reach at about 25Hz.

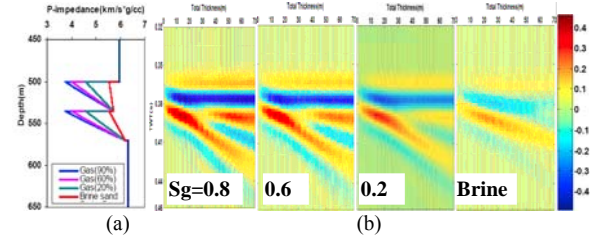


Figure 7. (a) P-impedance for the wedge models at four gas saturation conditions; (b) Synthetic seismic responses of the wedge models, where Sg is the gas saturation.

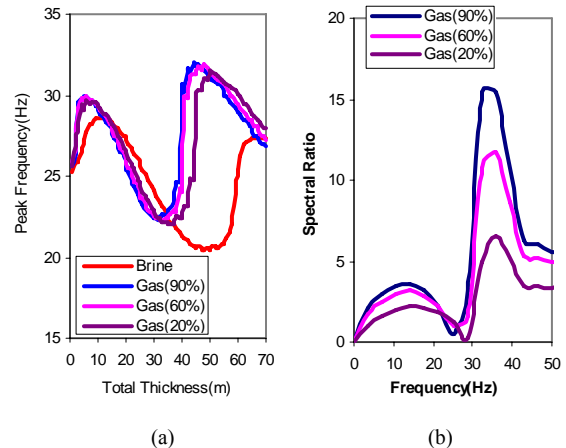


Figure 8. (a) Peak frequency versus total thickness for zero-degree incidence; (b) Spectral ratios between different gas saturation sand and brine sand at total thickness of 46m.

## Application of Spectral Decomposition to Detect Deepwater Gas Reservoir

Figure 9 shows iso-frequency sections from the stacked seismic data. Gas reservoir of Sand-2 cannot be separated from surrounding geology at low frequency about 10Hz, and exhibits weak anomalies at 14Hz. In 25Hz section, the spectral decomposition response of the sand reservoir and surrounding geology is similar, and no anomalies can be observed. At high frequency of 40Hz, the gas sand reservoir of Sand-2 stands out from surrounding geology, and shallow layers are also bright at such high frequency, which will deteriorate the likelihood to resolve the anomalies of deep reservoir from iso-frequency sections. The above spectral decomposition results agree well with the spectral ratio properties in Figure 8.

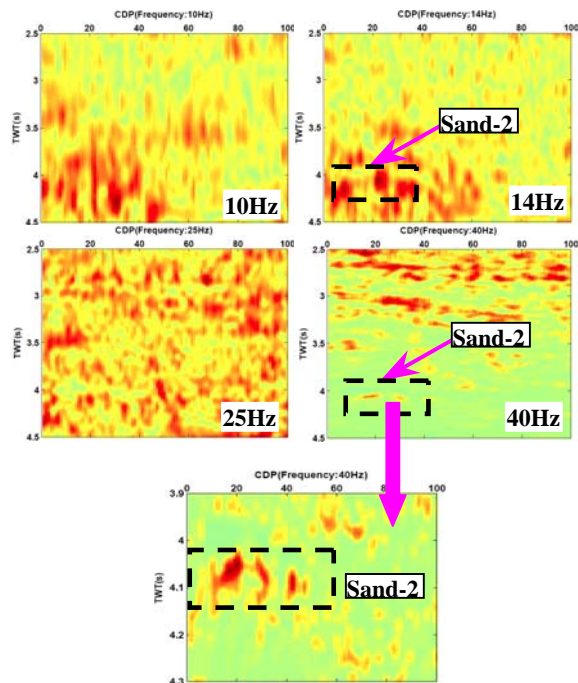


Figure 9. Selected monochromatic sections of the stacked seismic data of King Kong.

### Discussion and Conclusions

Applications of spectral decomposition techniques to stacked seismic section from deepwater reservoir show that gas associated spectral anomalies can occur at both low-frequency or high-frequency iso-frequency section. Analysis of the spectral attributes from synthetic forward model reveals that reservoir thickness and P-impedance structure are first order factors to control the spectral decomposition responses. In the first example, peak frequency of thick gas sand encased in shale with non-symmetric P-impedance shift to low frequency compared to

brine saturation, thus the spectral anomalies associated with gas can be observed in the low-frequency iso-frequency sections. In the second example, the peak frequency of gas reservoir with gradually changed P-impedance shift to high frequency, thus spectral anomalies of gas sand occur at high-frequency iso-frequency sections. Systematic synthetic model based on reservoir properties can provide information about the properties of spectral attributes for specific reservoir and aid in selecting optimal frequency range to detect hydrocarbon.

## EDITED REFERENCES

Note: This reference list is a copy-edited version of the reference list submitted by the author. Reference lists for the 2007 SEG Technical Program Expanded Abstracts have been copy edited so that references provided with the online metadata for each paper will achieve a high degree of linking to cited sources that appear on the Web.

## REFERENCES

- Batzle, M., and Z. Wang, 1992, Seismic properties of pore fluids: *Geophysics*, 57, 1369–1408.
- Castagna, J. P., and S. Sun, 2006, Comparison of spectral decomposition methods: *First Break*, 24, 75–79.
- Castagna, J. P., S. Sun, and R. W. Siegfried, 2003, Instantaneous spectral analysis: Detection of low-frequency shadows associated with hydrocarbons: *The Leading Edge*, 22, 120–127.
- Chen, G., C. Finn., R. Neelamani., and D. Gillard, 2006, Spectral decomposition response to reservoir fluids from a deepwater reservoir: 76th Annual International Meeting, SEG, Expanded Abstracts, 1665–1669.
- Chi, X., and D. Han, 2006, Fluid properties discrimination by AVO inversion: 76th Annual International Meeting, SEG, Expanded Abstracts, 2052–2056.
- Dvorkin, J., and M. Gutierrez, 2001, Textural sorting effect on elastic velocities: 71st Annual International Meeting, SEG, Expanded Abstracts, 1764–1767.
- Liu, J., and K. J. Marfurt, 2007, Instantaneous spectral attributes to detect channels: *Geophysics*, 72, no. 2, P23–P31.
- Partyka, G., J. Gridley, and J. Lopez, 1999, Interpretational applications of spectral decomposition in reservoir characterization: *The Leading Edge*, 18, 353–360.
- Stockwell, R. G., L. Mansinha, and R. P. Lowe, 1996, Localization of the complex spectrum: The S-Transform: *IEEE Transactions on Signal Processing*, 44, 998–1001.
- Zhao, B., H. Zhou., X. Li., and D. Han, 2006, Water saturation estimation using support vector machine: 76th Annual International Meeting, SEG, Expanded Abstracts, 1693–1697.